Phonon Angular Momentum Induced by the Temperature Gradient

Masato Hamada,[1] Emi Minamitani,[2] Motoaki Hirayama,[1,3,4] and Shuichi Murakami[1,3]

[1]*Department of Physics, Tokyo Institute of Technology, 2-12-1 Ookayama, Meguro-ku, Tokyo 152-8551, Japan*
[2]*Department of Materials Engineering, The University of Tokyo, 7-3-1 Hongo, Bunkyo-ku, Tokyo 113-8656, Japan*
[3]*TIES, Tokyo Institute of Technology, 2-12-1 Ookayama, Meguro-ku, Tokyo 152-8551, Japan*
[4]*Center for Emergent Mattar Science, RIKEN, 2-1 Hirosawa, Wako, Saitama 351-0198, Japan*

Phonon modes in crystals can have angular momenta in general. It nevertheless cancels in equilibrium when the time-reversal symmetry is preserved. In this Letter, we show that when a temperature gradient is applied and heat current flows in the crystal, the phonon distribution becomes off equilibrium, and a finite angular momentum is generated by the heat current. This mechanism is analogous to the Edelstein effect in electronic systems. This effect requires crystals with sufficiently low crystallographic symmetries, such as polar or chiral crystal structures. Because of the positive charges of the nuclei, this phonon angular momentum induces magnetization. In addition, when the crystal can freely rotate, this generated phonon angular momentum is converted to a rigid-body rotation of the crystal, due to the conservation of the total angular momentum. Furthermore, in metallic crystals, the phonon angular momentum will be partially converted into spin angular momentum of electrons.

DOI: 10.1103/PhysRevLett.121.175301

Conversions between the magnetization and the mechanical generation can be realized in various ways, such as the Einstein–de Haas effect [1] and Barnett effect [2]. In the Einstein–de Haas effect, when the sample is magnetized by the external magnetic field, the sample rotates due to the conservation of the angular momentum. On the other hand, in the Barnett effect, a rotation of the sample induces magnetization. The key mechanism of these effects is the spin-rotation coupling, which relates electronic spins with a mechanical rotation [3]. In addition, spin-rotation coupling also enables mechanical generation of spin current in various systems [4–6]. In these effects, rotational motions of phonons in solids are important, and in this context a phonon angular momentum is formulated theoretically [7–9].

Here, we focus on the phonon angular momentum introduced in [7], which represents rotational motions of the nuclei within each phonon mode. In crystals with time-reversal symmetry, i.e., those without magnetic field or magnetization, the phonon angular momentum of each mode is an odd function of the wave vector $\boldsymbol{k}$ and the total angular momentum vanishes in equilibrium due to cancellation between phonons with the wave vector $\boldsymbol{k}$ and those with $-\boldsymbol{k}$. Meanwhile, one can expect that this cancellation goes away by driving the system off the equilibrium, and nonzero phonon angular momentum is induced. In this Letter, to theoretically show this scenario, we consider a crystal with a finite heat current, and show a nonzero total phonon angular momentum in the crystal due to its nonequilibrium phonon distribution. The crystal symmetry should be sufficiently low to allow this effect, and in

particular the inversion symmetry should be absent. We calculate the phonon angular momentum generated by heat current for the wurtzite GaN as an example of polar systems and the Te (tellurium) and Se (selenium) as examples of chiral systems. For wurtzite GaN, we calculate the phonon properties by using the valence force field model and first-principles calculation, and for Te and Se, we calculate the phonon properties by using the first-principles calculation.

The phonon angular momentum [7] is a part of the angular momentum of the microscopic local rotations of the nuclei around their equilibrium positions. We begin with the eigenmode equation for phonons $D(\boldsymbol{k})\epsilon_\sigma(\boldsymbol{k}) = \omega_\sigma^2 \epsilon_\sigma(\boldsymbol{k})$, where $\epsilon_\sigma(\boldsymbol{k})$ is a displacement polarization vector at the wave vector $\boldsymbol{k}$ with a mode index σ, and D is the dynamical matrix. Here, we set the normalization condition as $\epsilon_\sigma^\dagger(\boldsymbol{k})\epsilon_\sigma(\boldsymbol{k}) = 1$. In equilibrium, the phonon angular momentum per unit volume [7] is expressed as

$$J_i^{\text{ph}} = \frac{1}{V}\sum_{\boldsymbol{k},\sigma} l_{\sigma,i}(\boldsymbol{k})\left[f_0(\omega_\sigma(\boldsymbol{k})) + \frac{1}{2}\right], \quad i = x, y, z, \quad (1)$$

$$l_{\sigma,i}(\boldsymbol{k}) = \hbar\epsilon_\sigma^\dagger(\boldsymbol{k})M_i\epsilon_\sigma(\boldsymbol{k}), \quad (2)$$

where $f_0(\omega_\sigma(\boldsymbol{k})) = 1/(e^{\hbar\omega_\sigma(\boldsymbol{k})/k_B T} - 1)$ is the Bose distribution function, $\omega_\sigma(\boldsymbol{k})$ is the eigenfrequency of each mode, T is the temperature, and V denotes the sample volume. The matrix M_i is the tensor product of the unit matrix and the generator of $SO(3)$ rotation for a unit cell with N atoms given by $(M_i)_{jk} = I_{N\times N} \otimes (-i)\varepsilon_{ijk}$ $(i, j, k = x, y, z)$. $\boldsymbol{l}_\sigma(\boldsymbol{k})$ in Eq. (2) is the phonon angular momentum of a mode σ at phonon wave vector $\boldsymbol{k}$. Because of the time-reversal
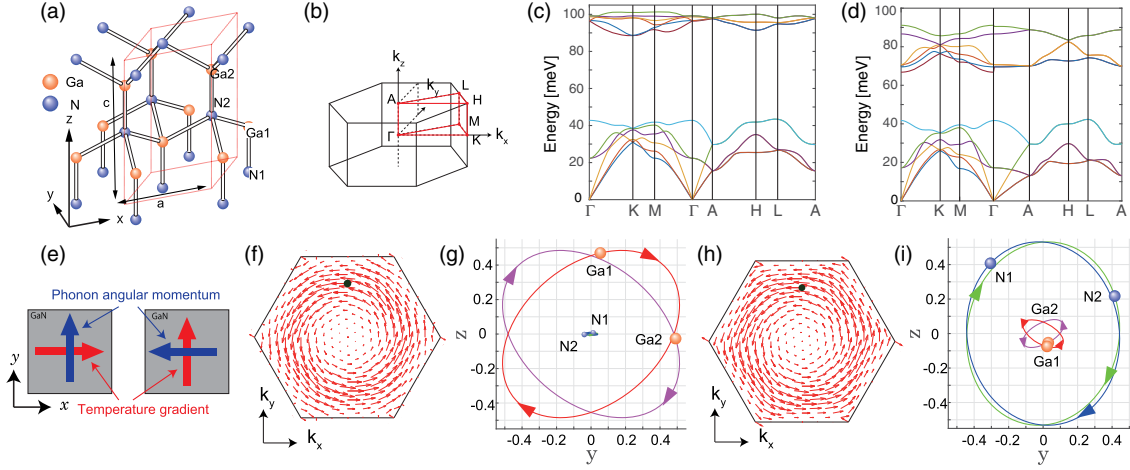
FIG. 1. Crystal structure of GaN, and phonon angular momentum of GaN. (a) Crystal structure of wurtzite GaN. The red line shows the unit cell. (b) First Brillouin zone of GaN. (c) Numerical results of phonon dispersion of wurtzite GaN using the valence force field model. (d) Numerical results of phonon dispersion of wurtzite GaN by first-principles calculation. (e) Schematic illustration of the relation between temperature gradient and the phonon angular momentum. (f) Distribution of the phonon angular momentum $l_\sigma(\mathbf{k})$ of the sixth lowest band on the plane $k_z = 0$. (g) Trajectories of the four atoms in the unit cell for the phonon of the sixth band at $(\mathbf{k}a/2\pi) = (0, 0.3849, 0)$, which is indicated as a black dot in (f). (h) Distribution of the phonon angular momentum $l_\sigma(\mathbf{k})$ of the eleventh lowest band on the plane $k_z = 0$. (i) Trajectories of the four atoms in the unit cell for the phonon of the eleventh band at $(\mathbf{k}a/2\pi) = (0, 0.3849, 0)$, which is indicated as a black dot in (h). (g) and (i) represent the normalized polarization vector $\varepsilon_\sigma(\mathbf{k})$ with $\varepsilon^\dagger \varepsilon = 1$, and their axes (x, y, z) are shown in a dimensionless unit.

symmetry of the system, it is an odd function of $\mathbf{k}$: $l_\sigma(\mathbf{k}) = -l_\sigma(-\mathbf{k})$, and their sum vanishes in equilibrium.

On the other hand, when the temperature gradient is nonzero, the phonon angular momentum becomes nonzero. Within the Boltzmann transport theory, the distribution function deviates from the Bose distribution function f_0 as

$$f_{\sigma,\mathbf{k}} = f_0(\omega_\sigma(\mathbf{k})) - \tau v_{\sigma,i}(\mathbf{k})\frac{\partial f_0}{\partial T}\frac{\partial T}{\partial x_i}, \qquad (3)$$

where $v_{\sigma,i}(\mathbf{k}) = \partial\omega_\sigma(\mathbf{k})/\partial k_i$ is the group velocity of each mode and x_i is the ith component of the position. To justify the use of the Boltzmann transport theory, we assume here that the deviation of the system away from equilibrium is small. In order to satisfy this condition, we focus on the linear response regime where the heat current is infinitesimally small. We also assume that the system relaxes towards the local thermal equilibrium quickly via nonlinear phonon-phonon interactions. As shown in Eq. (3), the effect of nonlinear phonon-phonon interactions is represented by the phonon relaxation time τ based on the constant relaxation time approximation. The dependence of τ on the mode index σ and the wave vector $\mathbf{k}$ does not alter our main conclusion and the constant relaxation time approximation is enough for a rough estimation. By substituting Eq. (3) into Eq. (1), the total phonon angular momentum per unit volume becomes

$$J_i^{\mathrm{ph}} = -\frac{\tau}{V}\sum_{\mathbf{k},\sigma}l_{\sigma,i}v_{\sigma,j}\frac{\partial f_0(\omega_\sigma(\mathbf{k}))}{\partial T}\frac{\partial T}{\partial x_j} \equiv \alpha_{ij}\frac{\partial T}{\partial x_j}, \quad (4)$$

where α_{ij} denotes a response tensor. The generated phonon angular momentum is proportional to the temperature gradient. This effect is caused by nonequilibrium phonon distribution, leading to an unbalance of phonon angular momentum, and therefore it is analogous to the Edelstein effect [10–16] in electronic systems.

In order to realize a nonzero response tensor α_{ij}, the crystal symmetry should be sufficiently low. Necessary conditions for the crystallographic symmetry are shown in the Supplemental Material [17]. It is instructive to decompose the response tensor into symmetric and antisymmetric parts. The antisymmetric part of α_{ij} is essentially a polar vector $\alpha_k \equiv \epsilon_{ijk}\alpha_{ij}$ and therefore it survives only for polar crystals, such as ferroelectrics and polar metals. In this case, when we set the z axis to be along the polarization or the polar axis, $\alpha_{xy} = -\alpha_{yx}$ are the only nonzero elements of this tensor. Thus, in any polar crystals, the temperature gradient and the generated angular momentum are perpendicular to each other, and they are both perpendicular to the polarization vector. On the other hand, the symmetric part of α_{ij} changes sign under inversion, and remains typically in chiral systems such as tellurium. In systems with very low symmetry, both the antisymmetric and the symmetric parts become nonzero.

As an example of polar systems, we discuss the wurtzite structure (space group: $P6_3mc$). The wurtzite structure has four atoms in the unit cell, as shown in Fig. 1(a) for GaN. When we take the polar axis to be along the z axis, the nonzero elements of the response tensor α_{ij} are $\alpha_{xy} = -\alpha_{yx}$ from symmetry analysis, as shown in Fig. 1(e). We first
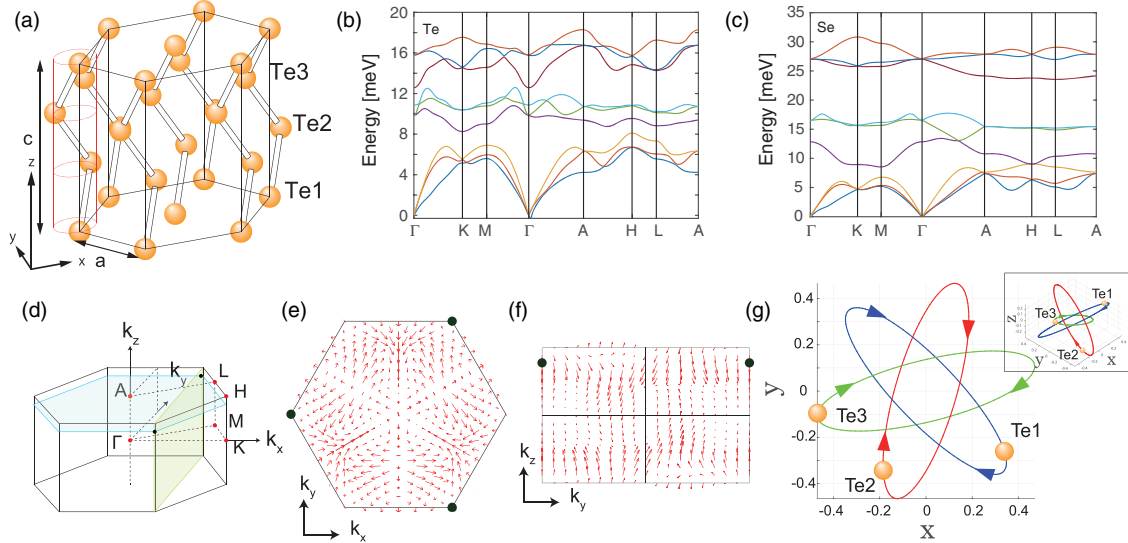
FIG. 2.   Phonon angular momentum of Te and Se in the first-principles calculation. (a) Crystal structure of Te. (b) Phonon dispersion of Te. (c) Phonon dispersion of Se. (d) First Brillouin zone of Te. (e),(f) Distribution of the phonon angular momentum $l_\sigma(\boldsymbol{k})$ of the fourth lowest band. (e) and (f) show the results on the plane $(k_z a/2\pi) = 0.2927$ and on the plane $(k_x a/2\pi) = \frac{1}{3}$, respectively. These planes correspond to the two cross sections in (d). (g) Trajectories of the four atoms in the unit cell for the phonon of the fourth lowest band at $(\boldsymbol{k}a/2\pi) = [\frac{1}{3}, (1/\sqrt{3}), 0.2927]$, which is indicated as the black dots in (d), (e), and (f). (g) represents the normalized polarization vector $\varepsilon_\sigma(\boldsymbol{k})$ with $\varepsilon^\dagger \varepsilon = 1$, and its axis (x, y, z) is shown in a dimensionless unit.

estimate the generated phonon angular momentum by heat current both by the valence force field model of Keating [26] and by first-principles calculations. We describe the details of our first-principles calculation in the Supplemental Material [17]. The lattice structure and corresponding Brillouin zone are shown in Figs. 1(a) and 1(b). The details of the valence force field model is summarized in the Supplemental Material [17]. The result of phonon dispersion for wurtzite GaN by the valence force field model calculation is Fig. 1(c). Despite its simplicity, this model well describes the nature of phonon and phonon angular momentum can be evaluated (see Supplemental Material [17]). The band structure obtained by the first-principles calculation [Figs. 1(d)] shows good agreement with previous works [27–29]. Overall features of the band structure are similar to those obtained by the valence force field model except for the splitting of the longitudinal and transverse optical bands at the long wavelength limit. Examples of distributions of phonon angular momentum $l_\sigma(\boldsymbol{k})$ are in Figs. 1(f) and 1(h), showing a similarity with spin structure in Rashba systems. We show the trajectories of atoms in the sixth and eleventh lowest modes in Figs. 1(g) and 1(i), respectively. By comparing Figs. 1(g) and 1(i), the oscillation of nitrogen atoms in the eleventh modes is much larger than that of the gallium atoms, while the oscillation of gallium atoms in the sixth mode is larger. The response tensor is estimated as $\alpha_{xy} \sim -10^{-7} \times [\tau/(1 \text{ s})] \text{ J s m}^{-2} \text{ K}^{-1}$ at $T = 300$ K.

As other examples, we consider Te (tellurium) and Se (selenium) [30]. Te and Se have a helical crystal structure, as shown in Fig. 2(a). The helical chains having three atoms

in a unit cell form a triangular lattice. The space group is $P3_121$ or $P3_221$ (D_3^4 or D_3^6) corresponding to the right-handed or left-handed screw symmetry. They are semi-conductors at ambient pressure. Numerical results of the phonon dispersions of Te and Se by first-principles calculation are shown in Figs. 2(b) and 2(c), respectively. The distributions of phonon angular momentum $l_\sigma(\boldsymbol{k})$ on the two planes in the Brillouin zone [Fig. 2(d)] are shown in Figs. 2(e) and 2(f) for the fourth lowest band. Because of the threefold screw symmetry around the z axis, the angular momentum on the k_z axis is along the z axis. Figure 2(g) represents the trajectories of the three atoms in the unit cell for the fourth mode. Here, because of the threefold screw symmetry at the $\boldsymbol{k}$ point considered, the trajectories are related with each other by threefold rotation around the z axis, and the angular momentum is along the z axis by symmetry. The overall features are similar between Se and Te, as shown in the Supplemental Material [17]. In Te and Se, from the symmetry argument, the response tensor has nonzero elements $\alpha_{xx} = \alpha_{yy}$ and α_{zz}, whose symmetry is identical with the electronic Edelstein effect in tellurium [16]. The response tensor for Te is estimated as $\alpha_{zz} \sim -10^{-7} \times [\tau_\parallel/(1 \text{ s})] \text{ J s m}^{-2} \text{ K}^{-1}$ and $\alpha_{xx} \sim 10^{-7} \times [\tau_\perp/(1 \text{ s})] \text{ J s m}^{-2} \text{ K}^{-1}$, and that for Se is estimated as $\alpha_{zz} \sim -10^{-6} \times [\tau_\parallel/(1 \text{ s})] \text{ J s m}^{-2} \text{ K}^{-1}$ and $\alpha_{xx} \sim -10^{-7} \times [\tau_\perp/(1 \text{ s})] \text{ J s m}^{-2} \text{ K}^{-1}$.

Next, we propose experiments to measure the phonon angular momentum generated by the heat current. The phonon angular momentum is a microscopic local rotation, and it cannot be measured directly. To measure this, we
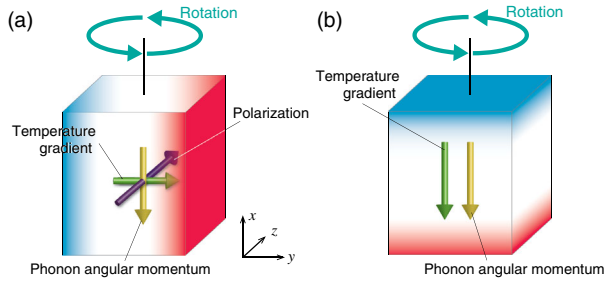
FIG. 3. Schematic diagram of the generated rigid-body rotation due to the heat current. (a) and (b) show two typical cases: (a) for a polar crystal such as wurtzite GaN and (b) for a chiral crystal such as Te and Se.

consider a phonon version of the Einstein–de Haas effect. Suppose the crystal can rotate freely. By conservation of angular momentum, when a heat current generates a phonon angular momentum J^{ph}, a rigid-body rotation of the crystal also acquires an angular momentum which compensates the phonon angular momentum, $J^{rigid\,body} = -J^{ph}$. This conservation holds when we take an average over a long period much longer than a typical timescale of the phonon motions, as discussed in detail in the Supplemental Material [17]. For example, in polar crystals, when the heat current flows along the y direction, the phonon angular momentum along the x direction is generated, and it is converted to a rigid-body rotation, as shown in Fig. 3(a). Similarly, in tellurium, it is schematically shown in Fig. 3(b), and the rotation direction will be opposite for right-handed and left-handed crystals. Next, we estimate the angular velocity ω of the rigid-body rotation in GaN as an example. We set the sample size to be $L \times L \times L$ and the phonon relaxation time to be $\tau \sim 10$ ps [29]. The temperature difference over the sample size L is denoted by ΔT. The angular momentum of the rigid-body rotation is represented as $J^{rigid\,body} L^3 = I\omega$, where $I = ML^2/6$ is the inertial moment of the sample with the total mass M. We estimate the angular velocity of the rigid-body rotation as

$$\omega = -J_x^{ph} L^3 / I \sim \frac{\Delta T/(1\mathrm{K})}{(L/(1\mathrm{m}))^3} \times 10^{-21}\ \mathrm{s}^{-1}. \qquad (5)$$

Then, by setting the temperature difference to be $\Delta T = 10$ K, an angular velocity of the rigid-body rotation ω is estimated as 10^{-8} s^{-1} when $L = 100$ μm and 10^{-2} s^{-1} when $L = 1$ μm. They are sufficiently large for experimental measurement. The estimations for Te and Se are shown in the Supplemental Material [17].

Because this phonon angular momentum means rotational motions of the nuclei having positive charges, it induces magnetization in itself. This can be estimated using a Born effective charge. The magnetic moment $\boldsymbol{m}$ is related with the angular momentum $\boldsymbol{j}$ by $\boldsymbol{m} = \gamma\boldsymbol{j}$ with the gyromagnetic ratio γ. In the case of wurtzite GaN, the Born effective charge tensor $eZ_{\alpha\beta}^*$ is $eZ_{xx}^* = eZ_{yy}^* = 2.58e$, $eZ_{zz}^* = 2.71e$ from our

ab initio calculation. The gyromagnetic ratio tensors of the Ga and N atoms are given by $\gamma_{\alpha\beta}^{Ga} = geZ_{\alpha\beta}^*/2m_{Ga}$ and $\gamma_{\alpha\beta}^N = -geZ_{\alpha\beta}^*/2m_N$ with a g factor of GaN $g_{\parallel} = 1.951$, $g_{\perp} = 1.9483$ [31], where m_{Ga} and m_N are the mass of the Ga atom and that of the N atom, respectively. We estimate the order of magnitude of the magnetization as

$$M_x \sim -\frac{\Delta T/(1\mathrm{K})}{L/(1\mathrm{m})} \times 10^{-11}\ \mathrm{A\,m}^{-1}. \qquad (6)$$

Therefore, the magnetization M_x of GaN induced by the temperature gradient is estimated as 10^{-6} A m^{-1} when $L = 100\,\mu$m, $\Delta T = 10$ K and 10^{-4} A m^{-1} when $L = 1\,\mu$m, $\Delta T = 10$ K. Although the order of magnitude of this magnetization is very small, it is expected to be observable experimentally.

In summary, we have theoretically predicted and estimated the phonon angular momentum generated by the heat current for wurtzite GaN, Te, and Se. This mechanism is analogous to the Edelstein effect in electronic systems. We proposed experiments to measure the phonon angular momentum generated by the heat current. When the crystals can rotate freely, the phonon angular momentum generated by heat current is converted to a rigid-body rotation of the crystals due to the conservation of angular momentum. This rigid-body rotation is sufficiently large for experimental measurement when the size of sample is micro order. On the other hand, because of the nuclei having a positive charge, the phonon angular momentum generated by heat current induces magnetization. Moreover, in metals, the phonon angular momentum will be partially converted to electronic spin angular momentum via the spin-rotation coupling, which is similar to the spin-current generation proposed for the surface acoustic waves in solids [5], and for the twiston modes in carbon nanotubes [6]. These experimental proposals are expected to unveil properties of the phonon angular momentum.

[1] A. Einstein and W. J. de Haas, Phys. Ges. **17**, 152 (1915).
[2] S. J. Barnett, Phys. Rev. **6**, 239 (1915).
[3] M. Matsuo, J. Ieda, E. Saitoh, and S. Maekawa, Phys. Rev. Lett. **106**, 076601 (2011).
[4] R. Takahashi, M. Matsuo, M. Ono, K. Harii, H. Chudo, S. Okayasu, J. Ieda, S. Takahashi, S. Maekawa, and E. Saitoh, Nat. Phys. **12**, 52 (2016).
[5] M. Matsuo, J. Ieda, K. Harii, E. Saitoh, and S. Maekawa, Phys. Rev. B **87**, 180402 (2013).

[6] M. Hamada, T. Yokoyama, and S. Murakami, Phys. Rev. B **92**, 060409 (2015).

[7] L. Zhang and Q. Niu, Phys. Rev. Lett. **112**, 085503 (2014).

[8] D. A. Garanin and E. M. Chudnovsky, Phys. Rev. B **92**, 024421 (2015).

[9] L. Zhang and Q. Niu, Phys. Rev. Lett. **115**, 115502 (2015).

[10] E. L. Ivchenko and G. E. Pikus, JETP Lett. **27**, 604 (1978).

[11] L. S. Levitov, Yu. V. Nazarov, and G. M. Eliashberg, Zh. Éksp. Teor. Fiz. **88**, 229 (1985) [Sov. Phys. JETP **61**, 133 (1985)].

[12] A. G. Aronov and Y. B. Lyanda-Geller, JETP Lett. **50**, 431 (1989).

[13] V. M. Edelstein, Solid State Commun. **73**, 233 (1990).

[14] J.-i. Inoue, G. E. W. Bauer, and L. W. Molenkamp, Phys. Rev. B **67**, 033104 (2003).

[15] Y. K. Kato, R. C. Myers, A. C. Gossard, and D. D. Awschalom, Phys. Rev. Lett. **93**, 176601 (2004).

[16] T. Yoda, T. Yokoyama, and S. Murakami, Sci. Rep. **5**, 12024 (2015).

[17] See Supplemental Material at http://link.aps.org/supplemental/10.1103/PhysRevLett.121.175301, which includes Refs. [18–25], for detailed discussion and details of calculations.

[18] R. R. Birss, *Symmetry and Magnetism, Series of Monographs on Selected Topics in Solid State Physics*, edited by E. P. Wohlfarth, Series of Monographs on Selected Topics in Solid State Physics Vol. 3 (Elsevier, North-Holland, 1962).

[19] S. Baroni, S. de Gironcoli, A. Dal Corso, and P. Giannozzi, Rev. Mod. Phys. **73**, 515 (2001).

[20] P. Giannozzi *et al.*, J. Phys. Condens. Matter **21**, 395502 (2009).

[21] K. F. Garrity, J. W. Bennett, K. M. Rabe, and D. Vanderbilt, Comput. Mater. Sci. **81**, 446 (2014).

[22] H. J. Monkhorst and J. D. Pack, Phys. Rev. B **13**, 5188 (1976).

[23] *The Physics of Selenium and Tellurium*, edited by W. C. Cooper (Pergamon, New York, 1969).

[24] *The Physics of Selenium and Tellurium*, edited by E. Gerlach and P. Grosse, Springer Series in Solid-State Sciences Vol. 13 (Springer-Verlag, Berlin Heidelberg, 1979).

[25] H. Peng, N. Kioussis, and D. A. Stewart, Appl. Phys. Lett. **107**, 251904 (2015).

[26] D. Camacho and Y. Niquet, Physica (Amsterdam) **42E**, 1361 (2010).

[27] T. Ruf, J. Serrano, M. Cardona, P. Pavone, M. Pabst, M. Krisch, M. D'Astuto, T. Suski, I. Grzegory, and M. Leszczynski, Phys. Rev. Lett. **86**, 906 (2001).

[28] C. Bungaro, K. Rapcewicz, and J. Bernholc, Phys. Rev. B **61**, 6720 (2000).

[29] X. Wu, J. Lee, V. Varshney, J. L. Wohlwend, A. K. Roy, and T. Luo, Sci. Rep. **6**, 22504 (2016).

[30] M. Hirayama, R. Okugawa, S. Ishibashi, S. Murakami, and T. Miyake, Phys. Rev. Lett. **114**, 206401 (2015).

[31] W. E. Carlos, J. A. Freitas, M. A. Khan, D. T. Olson, and J. N. Kuznia, Phys. Rev. B **48**, 17878 (1993).